



# Multi-objective optimization of FSW variables on joint properties of AA5754 aluminum alloy using Taguchi approach and grey relational analysis

Saleh S. Abdelhady<sup>1</sup> · Rehab E. Elbadawi<sup>2</sup> · Said H. Zoalfakar<sup>1</sup>

Received: 20 September 2023 / Accepted: 2 January 2024 / Published online: 15 January 2024  
© The Author(s) 2024

## Abstract

Friction stir welding (FSW) processing of the joint is a technique to improve the quality of the weld. The present research employed the friction stir welding technique to butt-weld AA5754 plates, whereby the joints of every weld case were identified based on their tensile strength, hardness, and impact toughness. The plates were joined by varying the rotational speeds, welding speeds, and tool tilt angles. A multi-objective optimization Taguchi's design of experiments approach and grey relational analysis (GRA) were used in this study to assess the combined effects of the process variables. The developed models are evaluated for sufficiency, and then the most significant parameters are determined using the analysis of variance (ANOVA). The results of the ANOVA showed that the rotational speed has a maximum contribution of 55.24%, 59%, and 46.27% in obtaining the optimal values of tensile strength, hardness, and impact toughness, respectively. It was found that formability and mechanical behaviors increased with increasing tilt angle for the tilt angle range examined in the current study. The two methods provide the same results, and the optimal conditions are a rotational speed of 1000 rpm, a welding speed of 60 mm/min, and a tilt angle of 2.5°. The optimal values for tensile strength, hardness, and impact toughness, respectively, were found to be 136 MPa, 85.25 HV, and 13 J. Significant implications for the welding industry may arise from the highly favorable outcomes in terms of microstructure and mechanical attributes.

**Keywords** Friction stir welding · Tensile strength · Taguchi method · Hardness · Grey relational analysis · Multi-objective optimization

## 1 Introduction

Aluminum alloys are prominent engineering materials with many industrial uses due to their strength and light weight [1]. Aluminum alloys from the 5xxx and 6xxx series are used to make automotive parts, while alloys from the 2xxx and 7xxx series are used to make aircraft structural parts [2, 3]. Friction stir welding is currently widely used in the welding of aluminum alloys because of its superior mechanical qualities [4–6]. A rotating, non-consumable tool with

a pin and shoulder is inserted into the joint line between the plates and moved along the joint line. This procedure produces frictional heat, which welds the junction. Friction stir processing and a new technique called friction stir vibration processing are used to process the weld area created by tungsten inert gas [7–9]. The process's maximum temperature increase is lower than the material's melting point. Because of this, the material does not provide any benefits over traditional fusion welding procedures, such as improved mechanical properties, reduced distortion, lower residual stresses, and fewer weld flaws [10].

The profile form and dimensions of the tool pin and tool shoulder of the welding tool have an impact on the rate of heat generation as well as the plastic flow of the workpiece during welding. Induced forces along the tool axis, heat generation per unit of time, and the flow of weld material on the workpiece are all directly influenced by the pin shape and surface characteristics like threads and tappers. [11, 12]. Therefore, constrained heating and material flow are

✉ Saleh S. Abdelhady  
salehgaballa@hotmail.com

<sup>1</sup> Department of Mechanical Engineering, Higher Technological Institute, 10Th of Ramadan City, P.O. Box: 228, Egypt

<sup>2</sup> Department of Mechanical Engineering, Mechatronics Engineering Program, Egyptian Academy for Engineering and Advanced Technology (EAEAT), Cairo City, Egypt

the two main functions of the tool, and the tool geometry has a significant role in determining both during the machining process (as well as the traverse rate) [13–16]. As a result, a key parameter that ensures proper joining during welding is the tool's rotation, traverse speed, angle, and shape [17]. At various tool traverse and rotational speeds, AA6061-T6 specimens were successfully fused together using conventional friction stir welding, friction stir vibration welding, and underwater friction stir welding [18].

The investigation focused on the impact of material location and tool deviation on the global and local mechanical behavior of friction stir-weld joints in aluminum alloys [19]. The flow of material during welding and the quantity of heat produced are both influenced by the tool's tilting angle. The interaction between the workpiece and tool shoulder, which encourages material flow across the tool, is confirmed by a little rise in the tool's tilt angle. Defective welds happen from a tool tilt angle that is too high because it elevates the pin from the weld's root. Therefore, choosing the right parameter settings is crucial to getting the best output results. The best parametric range settings are determined by doing a comprehensive literature review. Marathe et al.'s [20] studies on FSW of AA6061 plates used three different tool profiles, including square, tapered, and cylindrical. At a tool speed of 2750 rpm and a welding speed of 10 mm/min, tapered pins were used to produce the highest possible ultimate tensile strength. Devaiah et al. [21] discovered that the greatest Vickers microhardness value of 94.8 VHN was achieved when welding joints made of the dissimilar alloys 6.61 and 5083 at tool speeds of 1120 rpm, 70 mm/min, and 20 tool tilt angles. According to Panda et al. [22] hypothesis, welding AA6061 plates using a threaded cylindrical profile tool at 900 rpm and 60 mm/min produced a joint with an enhanced tensile strength of 160.7 MPa.

Taguchi technique applied to determine the best parameters for welding AA6061 and AA7075 aluminum alloys, and they concluded that 1000 rpm tool rotation, 110 mm/min traverse speed, and 30° of tool tilting produced the highest tensile strength [23]. To study the effects of process factors on mechanical strength and microstructural changes, Bhojan et al. [24] performed FSW on a hybrid aluminum composite. When welding AA2014-T651 and AA6063 T651, Ranjith [25] selected the tool offset, angle of tilt, and pin diameter as input parameters. The maximum tensile strength was 371 MPa using the values of 4° tool tilt angle, 0.5 mm offset towards advancing side, and 6-mm-pin diameter. For unlike non-ferrous aluminum alloy and titanium alloy, Palani and Elanchezhian [26] studied the effects of rotation speed, tool pin profiles, and welding speed on tensile strength, tensile elongation, and joint efficiency while utilizing FSW parameters. Following welding speed and the tool pin profiles discovered by ANOVA, rotation speed is the crucial factor in determining the quality of the welded joints. The Taguchi approach, which uses an orthogonal array of investigations, greatly reduces the variance for the experiment while

allowing for an optimal possible configuration of process control variables. To assess and optimize the welding parameters, the Taguchi methodology, a method for generating process improvements, was employed [27, 28]. By choosing the main variables that influence the process [29–31] and optimizing the methods to get the best results, these enhancements strive to improve the desirable features and reduce flaws. To examine the variation in the output responses, the input parameters are grouped and clustered in the L9 orthogonal array (OA) order [32, 33]. The Taguchi method was utilized to design the experiments and determine the optimal values for the welding parameters, including the effect of vibration, traverse welding speed, rotational speed, and welding tool tilt angle on the mechanical behavior and microstructure of AA6061-T6 alloy sheets [34].

Grey relational analysis was employed at different tool pin profiles, rotational speeds, and welding speeds to improve the medium grain particles at the nugget zone and durability, Santhanam et al. [35] introduced the friction stir welding alloy AA6063-O in mixed condition. Additionally, analysis of variance (ANOVA) is utilized to investigate the significance of process parameters for the mechanical properties and microstructure variability of both the standard FSW and mixed FSW joints. Ravikumar et al. [36] Optimization of unlike FSW joints between AA6061T-651 and AA7075T-651 aluminum alloys is calculated by ANOVA using grey relational grade from grey analysis and significant parameter contribution. Other parameters include rotation, welding velocity, pin profiles, ultimate tensile strength, and hardness. According to experimental findings, this unique technique is suitable for welding process responses. Raweni et al. [37] investigated the Taguchi design to optimize the set of parameters for FSW in terms of total fracture energy, crack initiation energy, and crack propagation energy in welds for rotating welding speed, traversing speed, and tool tilt angle. ANOVA was used to assess the effects of various parameters.

The literature research indicates that the FSW characteristics play an essential role in determining the quality of the joints. Additionally, the literature review shows that a large portion of research has been devoted to FSW single objective problem optimization of process parameters. Seldom has the optimization of process parameters by considering several mechanical characteristics been the subject of research. While some researchers recommended a square pin design, others suggested a cylindrical pin profile. Similarly, some researchers found that welding speed was the most critical component, while others found that rotational speed was an important contributing factor. Likewise, tool tilt angle was employed by earlier researchers, but it was considered an insignificant factor. Nevertheless, further research is still needed to determine how these process factors exactly affect the mechanical properties of AA5754. The literature review further demonstrates that the grey relational analysis (GRA) multicriteria decision-making approach is

**Table 1** Chemical composition (wt%) of AA5754 sheet

Element	Al	Mg	Mn	Fe	Si	Cu	Zn	Cr	Ti
wt%	Bal	2.6	0.50	0.40	0.40	0.10	0.20	0.30	0.15

**Table 2** Mechanical properties of AA5754 aluminum alloy

Ultimate tensile strength (MPa)	Percentage El. (%)	Vickers hardness (Hv)
236	27	44

an easy-to-use and efficient instrument for handling various objective situations. Thus, using the Taguchi approach and grey relational analysis, an attempt has been made in this investigation to maximize the tensile strength, hardness, and impact toughness in friction stir welded AA5754 aluminum alloy joints by optimizing a few important FSW parameters.

## 2 Materials and methods

### 2.1 Materials

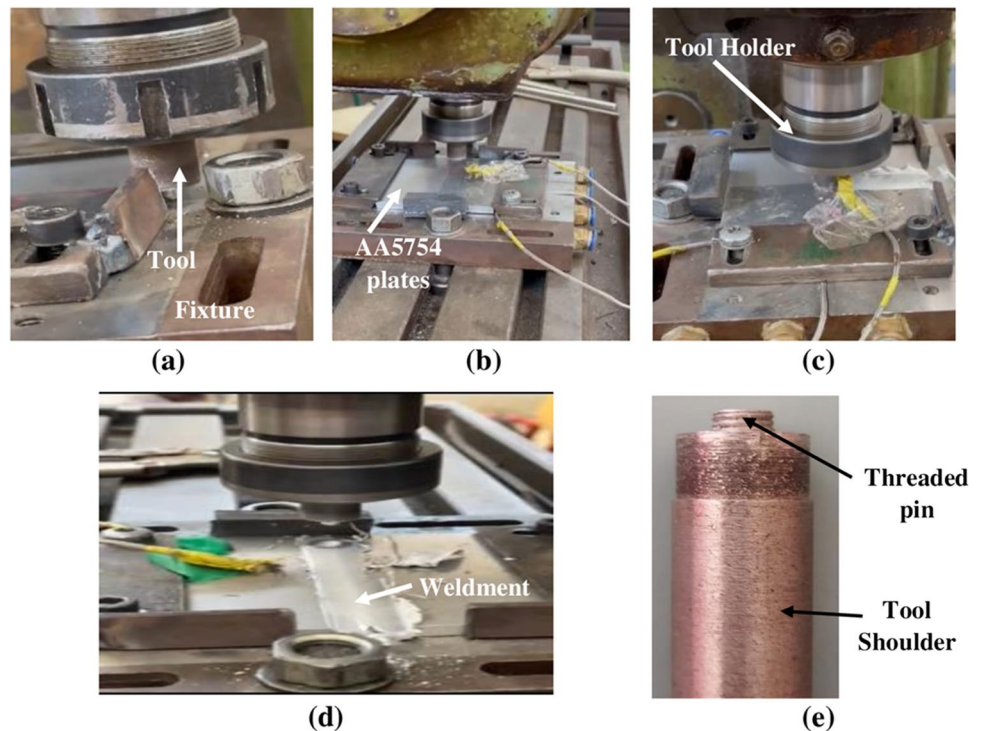
In this investigation, welding specimens with dimensions of  $100 \times 100 \times 6$  mm were cut from an AA5754 alloy plate. The chemical composition and mechanical properties of the AA5754 alloy are detailed in Table 1 and 2, respectively.

### 2.2 Friction stir welding process

The AA 5754 alloy plates are butt welded using the FSW process performed by a vertical milling machine. The plates were securely clamped using a specialized fixture (Fig. 1a). Pin tool plunging into the AA5754 plates (Fig. 1b). Figure 1c and d, respectively, show the travel of a tool along the joint line and its removal, once the weld is complete. A hardened H13 steel pin tool with a threaded pin profile of M6 mm, a height of 5 mm, and a shoulder diameter of 18 mm was utilized for this technique (Fig. 1e).

Following welding, the quality of the welded joint is evaluated using a variety of mechanical tests, including tensile, impact toughness, and hardness tests. The test samples were cut employing a wire cut electrical discharge machine into standard sizes in accordance with the ATSM standard. The tensile samples with a gauge length of 30 mm, a width of 6 mm, and a thickness of 6 mm have been trimmed perpendicular to the welded connection in accordance with ASTM E8 standard. Vickers' microhardness tester with a 100-g load and a 10-s dwell period was used to determine the microhardness of the FSW specimens. To assess the impact toughness of the weld joint, the Charpy impact test

**Fig. 1** Photographs of FSW procedure. **a** placing the tool and plates prior plunging, **b** pin tool plunging, **c** tool passing along a joint, **d** pin tool carrying away and eFSW tool



was performed. The V-notch sample (80 mm length, 10 mm width, and 6 mm thickness) for the Charpy test was constructed perpendicular to the welding connection, with the notch located in the middle of the connection. An optical microscope was used to carry out microstructural analysis. Before displaying the surface morphology of all samples, the surfaces were all ground and polished to a mirror-like finish. The samples were etched using Keller's reagent (3 ml HCl, 5 ml HNO<sub>3</sub>, 2 ml HF, and 175 ml distilled H<sub>2</sub>O) in accordance with ASTM E407 standard practice for micro etching metals and alloys. Scanning electron microscopy (SEM) Model Quanta 250FEG (field emission gun) was used to analyze joint fracture morphology.

### 2.3 Taguchi method

In the present investigation, the three process variables of tool rotation speed, welding speed, and tilt angle were conducted. The L<sub>9</sub> design of experiment by Taguchi was modified in this work to reduce the number of experiments. Table 3 depicts three variables and three levels of the control variables. The investigated input variable ranges have been identified from the literature, and Taguchi was used as the basis for designing the layouts of the various FSW experiments. The highest and lowest limits of the variables were selected to produce a weld free of defects [38, 39]. The L<sub>9</sub> orthogonal array was generated for three variables and levels, as shown in Table 4, and nine different arranged sets of tests were run applying this array.

The Taguchi technique employs a statistical performance metric known as the signal-to-noise (*S/N*) ratio to assess the process variables. As an objective function for optimization, the *S/N* ratio is a logarithmic function of the desired output [40, 41]. By evaluating the *S/N* ratio of the measured values, the optimal parameter combinations were identified. Each quality characteristic's *S/N* ratio can be calculated separately, and regardless of the performance characteristic category, a higher *S/N* ratio equates to higher quality characteristics. Nominal the best, Smaller the better, and Larger the better are the three categories for the commonly employed standard *S/N* ratios. In this study, the larger-the-better evaluation is employed to calculate the *S/N* ratio, which is defined by:

**Table 3** Design variables and their levels

Variables	Symbol	Units	Levels		
			1	2	3
Rotation speed	RS	rev/min	800	1000	1200
Travel speed	WS	mm/min	40	60	80
Tilt angle	TA	degree	1.5	2	2.5

**Table 4** The L<sub>9</sub> orthogonal array applied to the evaluations

Exp. no	Levels		
	Rotation speed (rev/min)	Travel speed (mm/min)	Tilt angle (°)
1	800	40	1.5
2	800	60	2
3	800	80	2.5
4	1000	40	2
5	1000	60	2.5
6	1000	80	1.5
7	1200	40	2.5
8	1200	60	1.5
9	1200	80	2

$$\text{Larger the better } S/N(\text{db}) = -10 \times \log_{10} \left( \frac{1}{n} \sum_{i=1}^n \frac{1}{y_i^2} \right) \quad (1)$$

where *n* is the number of evaluations, and *y* is the result of those observations of the *i*th performance characteristic. Also, the statistical technique analysis of variance (ANOVA) is used to examine the effects of different input parameters on establishing the levels of output responses in the weld joints. The ANOVA test is used to determine the significance of the process variables that affect the mechanical characteristics of weld junctions [42]. Additionally, by using the findings of the ANOVA, it is possible to estimate the influence of each parameter on the response.

### 2.4 GRA

Grey relational analysis (GRA) is the approach utilized when there are multiple attribute situations. With this approach, a grey relational grade (GRG) is used as the basis for the overall assessment of the multiple response procedure. Here, optimization is accomplished by reducing the complex numerous process values to a single GRG, and the best parametric combination that would produce the highest value of GRG is then assessed. To prepare the original data for analysis in the grey relational analysis, data preprocessing is first carried out. Normalization is a transformation carried out on a single data input to scale the data into an appropriate range and spread it uniformly for further analysis. In this research, the observed values are linearly normalized in the range between 0 and 1, also known as the grey relational generating range. The following formula normalizes  $[0 \leq X_i(\mathbf{K}) \leq 1]$ ,  $X_i(\mathbf{K})$  as to avoid the impact of using various units and to cut down on variability. According to the higher-is-better criterion, the normalized compressive strength can be represented as:

$$X_i(\mathbf{K}) = \frac{y_i(k) - \min y_i(k)}{\max y_i(k) - \min y_i(k)} \quad (2)$$

The frequency can be stated as, according to the lower-the-better criterion:

$$X_i(\mathbf{K}) = \frac{\max y_i(k) - y_i(k)}{\max y_i(k) - \min y_i(k)} \tag{3}$$

where  $X_i(\mathbf{K})$  denotes the value following the formation of the grey connection. The minimum value of  $y_i(k)$  for the  $k$ th response is  $\min y_i(k)$ , and the maximum value of  $y_i(k)$  for the  $k$ th response is  $\max y_i(k)$ .

The number of experiments is  $i = 1, 2, 3$ , and the number of replies is  $k = 1, 2, 3$ . The relationship between the reference sequence and the compatibility sequence is then determined by computing the grey relation coefficient (GRC). Equation (4) can be used to compute the GRC ( $\xi$ ) [36].

$$\xi = \frac{\Delta_{\min} + \delta \Delta_{\max}}{\Delta_i(k) + \delta \Delta_{\max}} \tag{4}$$

where,  $\Delta_{oi}(k) = |x_0(k) - x_i(k)|$  = difference between absolute value of  $x_0(k)$  and  $x_i(k)$ ;  $\psi$  is the distinguishing coefficient;  $0 \leq \delta \leq 1$  to provide replies equal preference in the present work, the value of  $\delta$  was chosen as 0.5 [43].  $\Delta_{\min}$  is the smallest value of  $\Delta_{oi}(k)$ , and  $\Delta_{\max}$  is the largest value of  $\Delta_{oi}(k)$ .

The GRG is a gauge of the relevance between two systems or two sequences. The grey relational coefficient for each performance trait is averaged to produce the GRG. The calculated GRG determines the multiple response process's total performance characteristic. The GRG is described as

$$\gamma_i = \frac{1}{m} \sum_{k=1}^m \xi_i(k) \tag{5}$$

where  $\bar{\gamma}_i$  is the mean GRG value at the desired level for the  $i$ th parameter;  $m$  is the number of process responses. The statistical significance of each component and the percentage contribution of each process parameter to the responses are also determined using the ANOVA approach.

### 3 Results and discussions

The best level of each process variable is determined using the signal-to-noise ratio ( $S/N$ ) ratio method to examine the results, which allows for the correlation of the highest  $S/N$  ratio and ensures the greatest value of the tensile strength, hardness, and impact toughness of the welded joints.

### 4 S/N evaluation

The Taguchi method was used to calculate the  $S/N$  ratio and estimate how each element will affect the process' output. One of the fundamental goals of the Taguchi approach is connected to the  $S/N$  ratio. It is used to assess quality characteristics and variation from actual values. As a result, the  $S/N$  ratio was used to identify the variable level that changes significantly and forecast the blending of the optimal procedure variables [44]. Furthermore, these parameters' effects on the mechanical properties of the AA5754 aluminum alloy were observed.  $S/N$  ratio at its highest value indicates that the process parameters are at their optimal level. The experimental data for tensile strength, hardness, impact toughness, and the associated  $S/N$  ratio, which were determined using Eq. (1), are shown in Table 5. According to the largest difference between values (delta statistics), each factor's effects (RS, WS, and TA) were ranked. As shown in Table 6, rotating speed, welding speed, and tilt angle were the welding parameters in decreasing order of significance for the tensile strength of the welded joints. Table 7 demonstrates that, in order of decreasing significance, rotating speed, welding speed, and tilt angle were the welding parameters for the hardness of the welded joints. Table 8 shows that the welding parameters for the impact toughness of the welded joints were rotating speed, welding speed, and tilt angle, in that order of decreasing significance.

**Table 5** Experimental results of tensile strength, hardness and impact toughness with their associated  $S/N$  ratios based on "larger is better"

Exp. no	Tensile strength (Mpa)	$S/N$ ratios (dB)	Hardness (HV)	$S/N$ ratios (dB)	Impact toughness (J)	$S/N$ ratios (dB)
1	106.00	40.5061	71.20	37.0496	5.00	13.9794
2	119.00	41.5109	76.00	37.6163	10.00	20.0000
3	115.50	41.2516	80.20	38.0835	8.00	18.0618
4	125.00	41.9382	82.10	38.2869	11.00	20.8279
5	136.50	42.7027	85.25	38.6139	13.00	22.2789
6	123.00	41.7981	84.10	38.4959	9.60	19.6454
7	113.25	41.0808	75.20	37.5244	7.80	17.8419
8	122.23	41.7436	81.20	38.1911	10.45	20.3823
9	124.00	41.8684	80.70	38.1375	9.00	19.0849

**Table 6** The means of tensile strength and estimated *S/N* response

Level	Means of tensile strength (Mpa)			Response for <i>S/N</i> ratios		TA
	RS	WS	TA	RS	WS	
1	113.5	114.8	117.1	41.09	41.18	41.35
2	128.2	125.9	122.7	42.15	41.99	41.77
3	119.8	120.8	121.8	41.56	41.64	41.68
Delta	14.7	11.2	5.6	1.06	0.81	0.42
Rank	1	2	3	1	2	3

**Table 7** The means of hardness and estimated *S/N* response

Level	Means of hardness (HV)			Response for <i>S/N</i> ratios		TA
	RS	WS	TA	RS	WS	
1	75.80	76.17	78.83	37.58	37.62	37.91
2	83.82	80.82	79.60	38.47	38.14	38.01
3	79.03	81.67	80.22	37.95	38.24	38.07
Delta	8.02	5.50	1.38	0.88	0.62	0.16
Rank	1	2	3	1	2	3

**Table 8** The means of impact toughness and estimated *S/N* response

Level	Means of impact toughness (J)			Response for <i>S/N</i> ratios		TA
	RS	WS	TA	RS	WS	
1	7.667	7.933	8.350	17.35	17.55	18.00
2	11.200	11.150	10.000	20.92	20.89	19.97
3	9.083	8.867	9.600	19.10	18.93	19.39
Delta	3.533	3.217	1.650	3.57	3.34	1.97
Rank	1	2	3	1	2	3

**Table 9** Analysis of variance for tensile strength

Symbol	Welding variables	<i>DF</i>	Adj <i>SS</i>	Adj <i>MS</i>	<i>F</i> -value	Contribution (%)
RS	Rotational speed	2	324.69	162.35	14.85	55.24
WS	Welding speed	2	187.33	93.66	8.57	31.87
TA	Tilt angle	2	53.93	26.96	2.47	9.17
Error		2	21.86	10.93		3.72
Total		8	587.81			100

#### 4.1 Analysis of variance

The analysis of variance (ANOVA) method is used to investigate the significant impacts of controllable factors and their interactions with one another. As a result, it is possible to determine the optimal (optimum) level settings for controllable elements by screening them first and then ranking them using ANOVA [45, 46]. Tables 9, 10, and 11 reveal, respectively, the percentage contribution to tensile strength, hardness, and impact toughness of the tool rotation speed, welding speed, and tilt angle. The contribution percentage represents the relative ability of a component to lessen variation and is a function of

the sum of squares (*SS*) for each significant variable. The significant influence on the process' responses is demonstrated by the high contribution value for this variable. In this investigation, the weld process responses are significantly influenced by the tool rotational speed (*RS*) and welding speed (*WS*), both of which are extremely significant variables. According to ANOVA Table 9, the rotating speed (*RS*) is the most important variable, contributing 55.24% to the peak tensile strength of the friction stir welded material. The next two variables that affect tensile strength are welding speed (*WS*) and tilt angle (*TA*), which contribute 31.87% and 9.17%, respectively. The tool rotational speed is an extremely significant

**Table 10** Analysis of variance for hardness

Symbol	Welding variables	DF	Adj SS	Adj MS	F-value	Contribution (%)
RS	Rotational speed	2	97.602	48.801	7.91	59
WS	Welding speed	2	52.595	26.298	4.27	31.8
TA	Tilt angle	2	2.882	1.441	0.23	1.74
Error		2	12.332	6.166		7.46
Total		8	165.410			100

**Table 11** Analysis of variance for impact toughness

Symbol	Welding variables	DF	Adj SS	Adj MS	F-value	Contribution (%)
RS	Rotational speed	2	18.972	9.4858	16.47	46.27
WS	Welding speed	2	16.432	8.2158	14.27	40.08
TA	Tilt angle	2	4.445	2.2225	3.86	10.84
Error		2	1.152	0.5758		2.81
Total		8	41.000			100

variable for hardness, accounting for 59% of the overall variation, as indicated in Table 10. The next contribution to hardness results in 31.8% and 1.74%, respectively, of the welding speed and tilt angle. As shown in Table 11, the tool rotational speed significantly influences impact toughness, accounting for 46.27% of the total variation. The following two variables, which are welding speed and tilt angle, each contribute 40.08% and 10.84% to impact toughness, respectively.

### 4.2 Development of linear and multiple regression model

A mathematical relationship between the independent and dependent variables can be established following the ANOVA analysis to estimate the tensile strength, hardness, and impact toughness of the joints manufactured by the FSW procedure. The linear regression model is written as:

$$Y = f(RS, WS, TA) \tag{6}$$

where  $Y$  is the objective function; RS is the rotational tool speed; WS is the welding speed; and TA is the tilt angle. The selected polynomial can be represented as follows for all three variables:

$$Y = \beta_0 + \beta_1(RS) + \beta_2(WS) + \beta_3(TA) + \beta_4(RS \times WS) + \beta_5(RS \times TA) + \beta_6(WS \times TA) \tag{7}$$

where  $\beta_0$  is a constant;  $\beta_1, \beta_2,$  and  $\beta_3$  are the linear term coefficients.  $\beta_4, \beta_5,$  and  $\beta_6$  are the coefficients of the interaction terms.

Develop the first order polynomial equation shown below based on the results of the multiple regression analysis of the design matrix and the response values:

$$\begin{aligned} \text{Tensilestrength(Mpa)} = & 120.50 - 7.00RS\_1 + 7.67RS\_2 \\ & - 0.67RS\_3 - 5.75WS\_1 + 5.41WS\_2 \\ & + 0.34WS\_3 - 3.42TA\_1 + 2.17TA\_2 \\ & + 1.25TA\_3 \end{aligned} \tag{8}$$

$$\begin{aligned} \text{Hardness(HV)} = & 79.550 - 3.75RS\_1 + 4.27RS\_2 - 0.52RS\_3 \\ & - 3.38WS\_1 + 1.27WS\_2 + 2.12WS\_3 \\ & - 0.72TA\_1 + 0.05TA\_2 + 0.67TA\_3 \end{aligned} \tag{9}$$

$$\begin{aligned} \text{Impact(J)} = & 9.317 - 1.650RS\_1 + 1.883RS\_2 - 0.233RS\_3 \\ & - 1.383WS\_1 + 1.833WS\_2 - 0.450WS\_3 \\ & - 0.967TA\_1 + 0.683TA\_2 + 0.283 \end{aligned} \tag{10}$$

The significance of the adjustment for the means Eqs. (8), (9), and (10) of the tensile strength, hardness, and impact toughness, respectively, is examined using the ANOVA analysis presented in abovementioned Table 9, 10, and 11. The coefficient of determination ( $R-Sq=96.3\%, 92.5\%$ , and  $97.2\%$  for tensile strength, hardness, and impact toughness, respectively) has a greater value in the model than the adjusted coefficient of determination ( $R-Sq(adj)=95.8\%, 91.5\%$ , and  $96.8\%$  for tensile strength, hardness, and impact toughness, respectively), indicating a strong correlation between the predicted values and the actual results of the experiment. A diagonal line in Fig. 2 depicts the predicted values against the experimental values, showing a uniform random distribution of all the points with a linear correlation. As a result, the

model that was developed is deemed adequate and predicts the response with reasonable errors.

### 4.3 Evaluation of experimental results

The main effects plot for tensile strength is displayed in Fig. 3 a. At the extreme levels 1 and 3, the mean tensile strength is low, while at level 2, it is at its highest. While the rotational speed (RS) gets higher to the middle level (1000 rpm) and then drops, the tensile strength of the weld improves. The highest effect is at the intermediate level (60 mm/min) and is also influenced by welding speed (WS), which has a comparable effect. Weld speed and tool rotational speed typically rise as they generate more heat, which has a greater impact on the tensile strength [47, 48]. The frictional heating and plastic deformation of the material are caused by the rotational speed, which results in mixing and churning of the material around the pin. In addition to the increased friction heating caused by faster tool rotation rates, the material is stirred and mixed more vigorously. Tensile strength drops because of the FSW

thermal cycle's peak temperature rising because it produces large, recrystallized grains, exceptional grain growth, and dissolved precipitates [49].

Figure 3 b displays the hardness main effects plot. The weld zone hardness increases as the rotational speed (RS) rises to a midway level (1000 rpm), then declines. The production of coarse grain structure at the weld zone is caused by the increased heat generation at higher tool rotating speeds, which causes more heat to dissipate to the workpiece. This lessens the weld zone's hardness [50, 51]. The amount of material deformation and frictional heat are reduced as welding speed is increased. According to the general principles of recrystallization, the reduction of the deformation degree prevents dynamic recrystallization, increasing the recrystallized grain size and raising the hardness of the weld zone as the welding speed increases [52, 53]. Also, it can be shown in Fig. 3 c that the mean impact toughness is lowest at levels 1 and 3 and highest at level 2, respectively. The impact toughness also rises with rotational speed and welding speed. At tool rotational speeds of

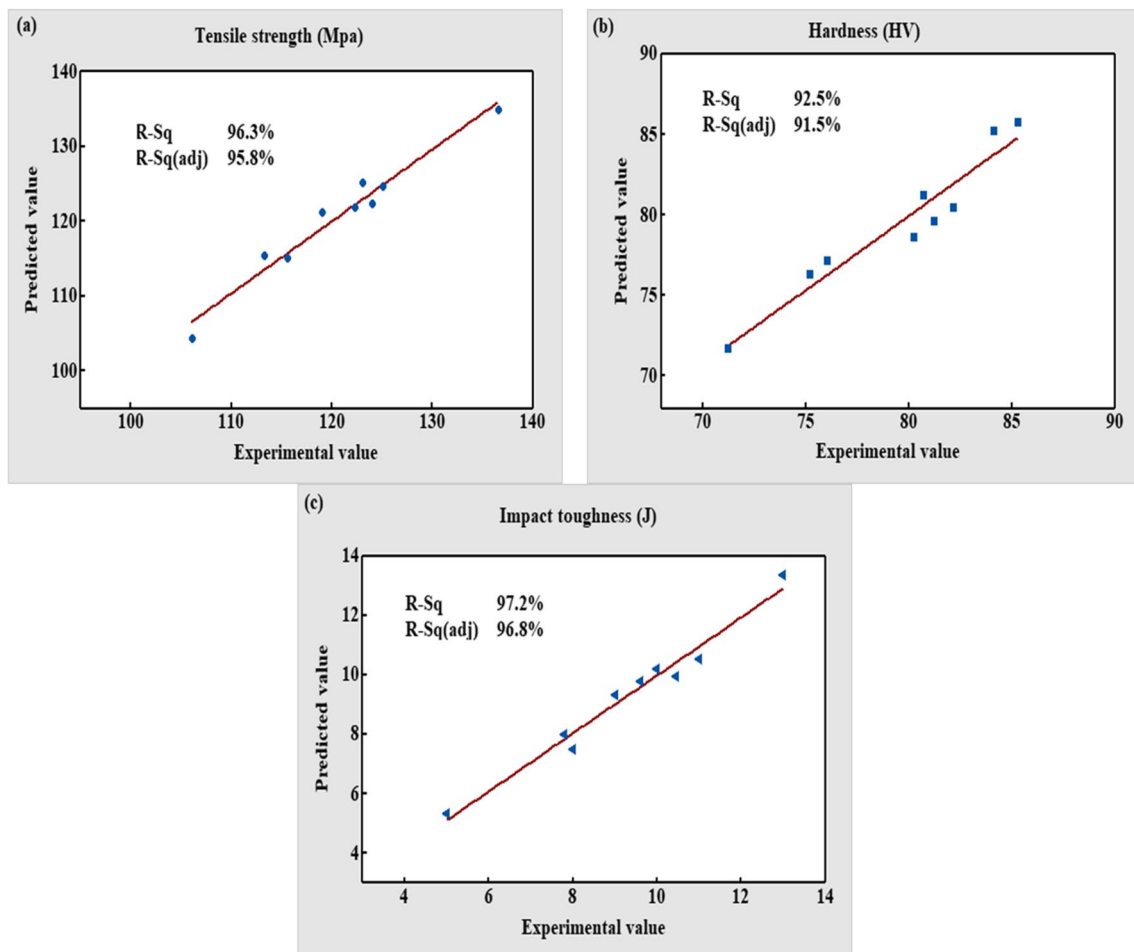
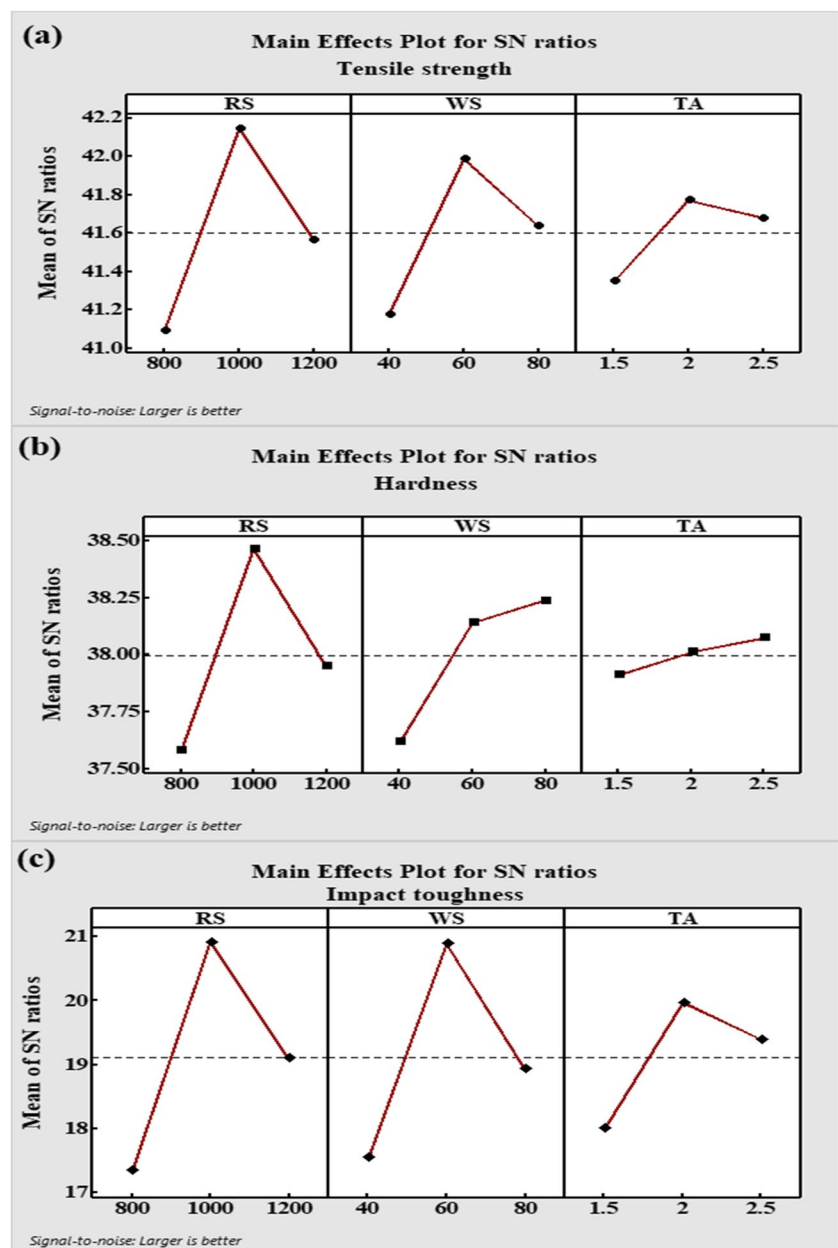


**Fig. 2** Relationship between predicted and experimental values for all responses **a** tensile strength, **b** hardness, and **c** impact toughness



**Fig. 3** Response graph for procedure variables effects on tensile strength (a), hardness (b), and impact toughness (c)



800 rpm and 1200 rpm, the impact toughness and tensile strength are lowest, while at 1000 rpm, they are at their highest. Additionally, 60 mm/min weld speed created greater values of impact toughness and tensile strength while the weld speeds (40 and 80 mm/min) have produced lower values.

The tilt angle (TA) has a substantial impact on the material flow. A higher tilt angle increased the frictional force at the tool/workpiece interface, which significantly increased the velocity of the material flow behind the tool. Tool tilt angle influenced the joint tensile and impact toughness, and a substantially parabolic type of variation was seen against the tool tilt angle (the joint strength initially rises, reaches a maximum, and then drops up on increases in tool

tilt angle) [54]. Additionally, at greater tool tilt angles, the plunge depth becomes shallower, reducing the amount of base material that the rotating tool shoulder can effectively contact, reducing the amount of plasticized material that can be transferred from the front to the back of the tool, and reducing the strength of the weld joint. Dynamic recrystallization, which took place during the welding process as tilt angle increased due to an increase in total heat generation and the extrusion of base metals into the weld zone, is responsible for the increase in the hardness values in the weld zone [55]. The weld zone's relative improvement in hardness with increasing tilt angle is due to the recrystallized grain size that produced the fine grain structure.

The input factors are optimized using regression modeling to get the highest tensile strength, hardness, and impact toughness. Figure 4 displays the optimal input values for variables for the highest tensile strength, hardness, and impact toughness. The model predicts that the optimized composite will have a tensile strength of 136 MPa, a hardness of 85 HV, and an impact toughness of 13 J, which will be obtained by fabricating it at 1000 rpm rotational speed, 60 mm/min welding speed, and a tilted angle of 2.5°. The optimum welding parameter values rely on the strength, thermal conductivity, and melting point of the individual materials that are being fused together. As a result, it is impossible to present the best welding conditions for various materials [56].

#### 4.4 Taguchi approach evaluation of the GRG with variables

Taguchi established an approach determined by an orthogonal array of experiments that significantly reduces experiment variation when process control variables are set to their optimal values. The Taguchi technique applies a statistical measure of performance known as the signal-to-noise ( $S/N$ ) ratio to assess the process variables. Multi-objective optimization problems, however, cannot be optimized using the conventional Taguchi method. The Taguchi approach and grey relational analysis (GRA) are employed for optimizing multi-objective problems to get around this. Multi-objective optimization problems are reduced to single-objective issues using the grey relational analysis method. The optimal variable combination is then assessed. As a result, the largest grey relational grade (GRG) is acquired [57, 58]. The data (means) are normalized into a comparable sequence in

the range of 0 to 1 pursuant to the GRA approach. Table 12 provides the normalized values of each response as determined by Eq. (2). These normalized values are employed to determine the grey relational coefficient of each output response applying Eq. (4), (Table 13). Subsequently, the grey relational grade for each experiment is determined by averaging the grey relational coefficient using Eq. (5) and is also shown in Table (13). The result shows that experiment 5 has greater tensile strength, hardness, and impact toughness, as it has the largest grey relational grade of 1 within the nine investigations.

Based on the experimental findings, a comprehensive factor analysis of GRG and  $S/N$  ratio is carried out. The response for GRG means and  $S/N$  ratio means are shown in Table 14. The rotational speed, followed by the welding speed and the tilt angle, was shown to have the greatest influence on the GRG and  $S/N$  ratios.

#### 4.5 ANOVA analysis for GRG

Analysis of variance has been used for examining significant procedure variables and the corresponding percentage contributions to the GRG of FSW joints. The effect of every variable on GRG gets clearly assessed using findings of an ANOVA. The GRG ANOVA analysis is presented in Table 15. Table 15 demonstrates that the variable RS, which has the largest contribution to the overall variability (59.83%), is followed by the variables WS (27.26%) and TA (6.39%).

Develop the following first order polynomial equation after doing ANOVA, multiple regression analysis, and response values (GRG):

**Fig. 4** Optimum variables for maximum tensile strength, hardness, and impact toughness

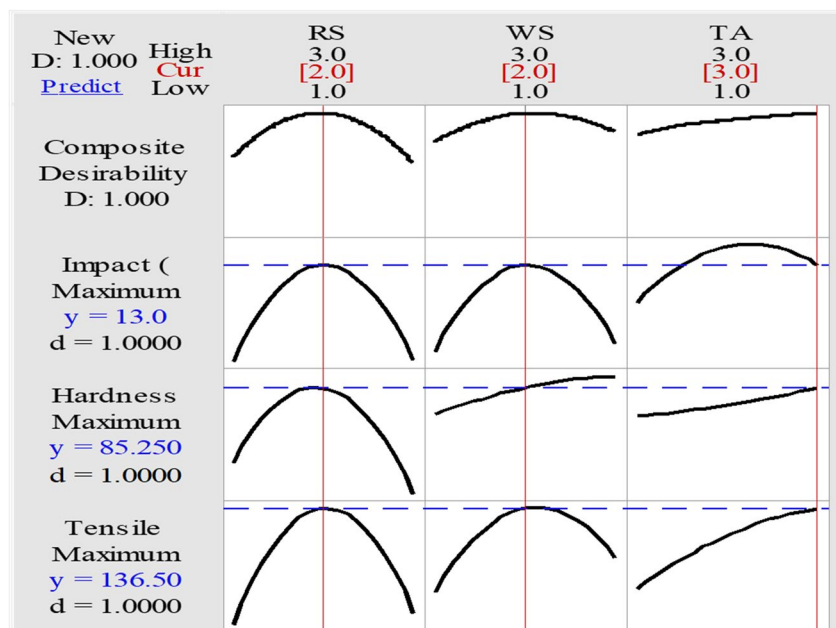


**Table 12** Estimation of normalized data for each response and deviation coefficients

Exp. no	Normalized data ( $X_i(K)$ )			Deviation coefficients( $\Delta io$ )		
	Tensile strength	Hardness	Impact toughness	Tensile strength	Hardness	Impact toughness
1	0	0	0	1	1	1
2	0.433	0.342	0.625	0.567	0.658	0.375
3	0.317	0.641	0.375	0.683	0.359	0.625
4	0.633	0.776	0.75	0.367	0.224	0.25
5	1	1	1	0	0	0
6	0.567	0.918	0.575	0.433	0.082	0.425
7	0.242	0.285	0.35	0.758	0.715	0.65
8	0.541	0.712	0.681	0.459	0.288	0.319
9	0.6	0.676	0.5	0.4	0.324	0.5

**Table 13** Grey relational coefficient, grey relational grade, and *S/N* ratios

Exp. no	Grey relational coefficient ( $\xi_i(k)$ )			Grey relational grade ( $\gamma_i$ )	<i>S/N</i> ratios (db)
	Tensile strength	Hardness	Impact toughness		
1	0.333	0.333	0.333	0.333	−9.54243
2	0.469	0.432	0.571	0.491	−6.18533
3	0.423	0.582	0.444	0.483	−6.32250
4	0.577	0.690	0.667	0.645	−3.81326
5	1	1	1	1	0.00000
6	0.536	0.859	0.540	0.645	−3.80619
7	0.397	0.411	0.435	0.415	−7.64913
8	0.521	0.634	0.611	0.589	−4.60076
9	0.556	0.607	0.5	0.554	−5.12736

**Table 14** The means of GRG and estimated *S/N* response

Level	Means of GRG			Response for <i>S/N</i> ratios		TA
	RS	WS	TA	RS	WS	
1	0.4356	0.4642	0.5224	−7.350	−7.002	−5.983
2	0.7633	0.6931	0.5631	−2.540	−3.595	−5.042
3	0.5192	0.5608	0.6325	−5.792	−5.085	−4.657
Delta	0.3277	0.2290	0.1100	4.810	3.406	1.326
Rank	1	2	3	1	2	3

**Table 15** Analysis of variance for GRG

Symbol	Welding variables	<i>DF</i>	Adj <i>SS</i>	Adj <i>MS</i>	<i>F</i> -value	Contribution (%)
RS	Rotational speed	2	0.17394	0.086972	9.18	59.83
WS	Welding speed	2	0.07927	0.039637	4.18	27.26
TA	Tilt angle	2	0.01857	0.009286	0.98	6.39
Error		2	0.01895	0.009474		6.52
Total		8	0.29074			100

$$\begin{aligned}
 \text{GRG} = & 0.5727 - 0.1371\text{RS}_1 + 0.1906\text{RS}_2 - 0.0535\text{RS}_3 \\
 & - 0.1085\text{WS}_1 + 0.1204\text{WS}_2 - 0.0119\text{WS}_3 \\
 & - 0.0502\text{TA}_1 - 0.0095\text{TA}_2 + 0.0598\text{TA}_3
 \end{aligned}
 \tag{11}$$

The coefficient of determination (*R-Sq*) is used to evaluate a model’s suitability and serves as an indicator

for the model’s strength, since it includes both significant and non-significant variables, whereas *R-Sq*(adj) is just related to significant variables. Therefore, *R-Sq*(adj) value is always less than or equal to *R-Sq* value. The model developed for GRG has an *R-Sq* and *R-Sq*(adj) of 93.48% and 92.55%, respectively.

#### 4.6 The optimal value for each variable

Applying the estimated GRG values (Table 13), the mean effect for each level of the parameters was calculated (Table 14). Moreover, Fig. 5 exhibits the main effects of the grey relational grade. Providing the largest GRG value for each factor, the optimal condition is attained at 1000 rpm for rotating speed (RS), 60 mm/min for welding speed (WS), and 2.5° for tilt angle (TA). The depicted optimal welding condition is obviously one of the conditions in

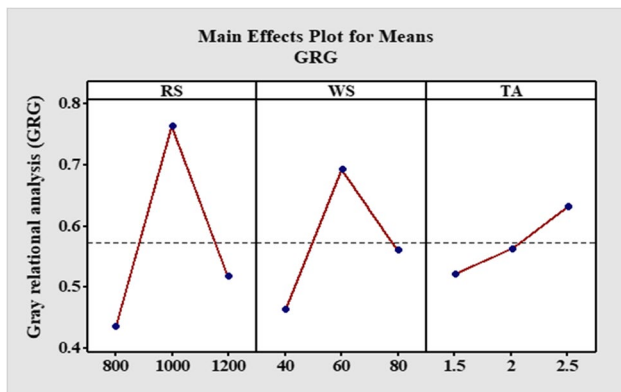
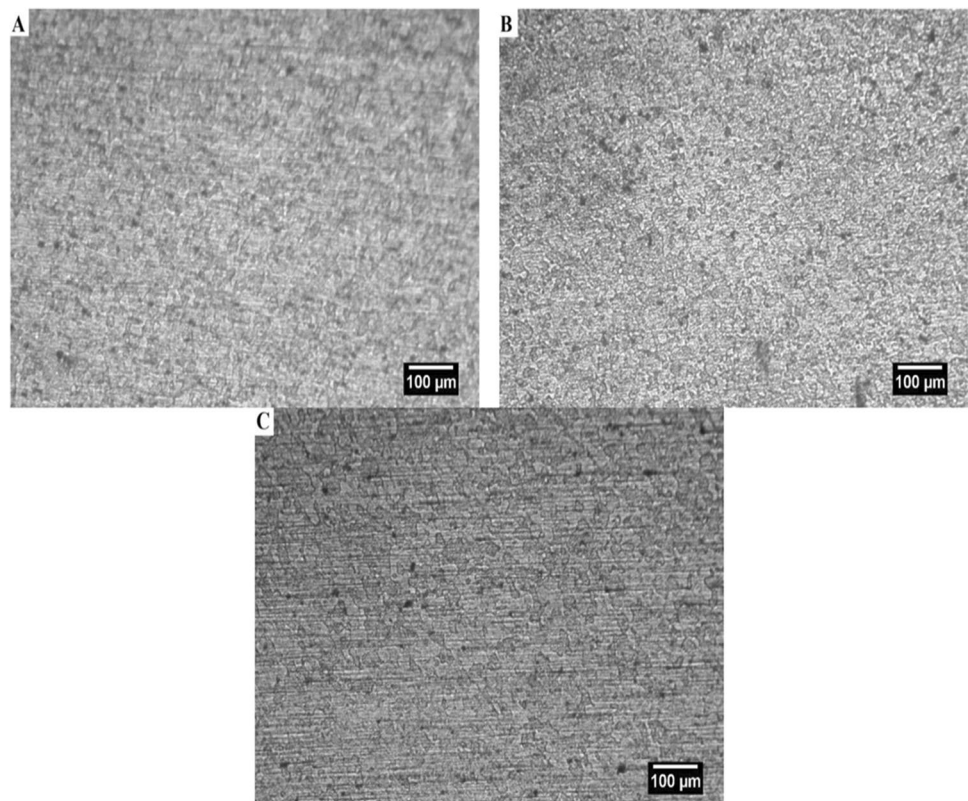


Fig. 5 Response graph for procedure variables effects on GRG

Fig. 6 Microstructural evaluation of the stir zone at **a** 1000 rpm, 40 mm/min, 2° (exp.#4); **b** 1000 rpm, 60 mm/min, 2.5° (exp.#5); and **c** 1000 rpm, 80 mm/min, 1.5° (exp.#6)



the orthogonal experimental design. This state denotes the maximum values for tensile strength, hardness, and impact toughness.

#### 4.7 The microstructural evaluation of the stir zone

Figure 6 exhibits the optical microstructures of the stir zone of the FSW joints (exp.#4, exp.#5, and exp.#6). As a result of the dynamic recrystallization process, the stir zone in each experiment has roughly equiaxed fine grains [59]. Moreover, it has been recognized that dynamic recrystallization occurs during FSW, generating fine, equiaxed grains in the stir zone. It is obvious that when welding speed and tilt angle increase, the size of the stirred zone grains reduces at a constant rotational speed (Fig. 6a, b) [60]. The dynamic recrystallization phenomenon might be associated with the smaller grain size in the stir zone (SZ). High-density dislocation during FSW is caused by severe plastic deformation [61]. Furthermore, it implies that in the FSW, strong plastic deformation splits the original grains and forms low angle, wrongly oriented grain boundaries, which promotes the development of a sizable number of nucleating zones for recrystallization [62–64]. Additionally, as welding speed is increased further and the tilt angle is decreased, the area of the stirred zone is reduced, increasing grain size (Fig. 6c). This might be explained by the welding tool not having enough time to completely stir the material. Greater heat generation at tool tilt of 1.5° was

the cause of the slightly larger grains in the stir zone. However, when tilt angles increased, the reduction in grain size became more apparent since at  $2^\circ$  and  $2.5^\circ$  tool tilt degrees, heat generation dropped as material strain rate increased [65]. Additionally, changes in welding speed have greater effects on changes in grain size and precipitation behavior. The joint was constructed utilizing a reduced tool traverse speed, which led to a large heat input because of the lengthy stirring time. As a result, joints made using lower welding speeds had greater grain sizes than joints made using higher welding speeds.

#### 4.8 Surface evaluation of fractures

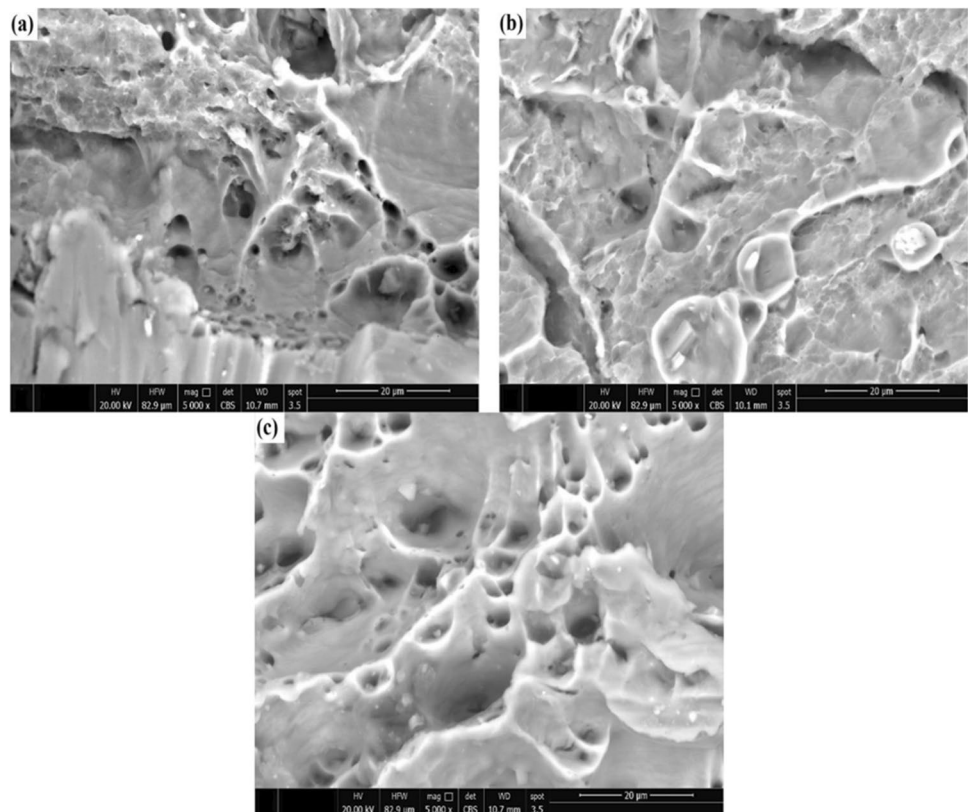
Figure 7 represents the tensile fractured surface. The weakest part of a welded joint is indicated by the fracture position. Fracture sites are an indicator of the distribution of strength for a joint without defects [66]. In contrast, the FSW joint has both large and small dimples. All specimens have a ductile fracture, as indicated by the presence of dimples [67]. A mixed-type fracture with ductile fracture features and grain boundary segregation was visible in the fractography of the joints. Dimples were found that were sparsely populated and devoid of voids, indicating a joint that was free of defects and had a typical fracture.

## 5 Conclusion

In the present investigation, AA5757 alloy plates were joined by FSW. The optimal values of the welding variables, which include rotational speed, welding speed, and tilt angle, were determined based on tensile, hardness, and impact toughness results by applying Taguchi method and grey relational analysis. According on the present investigation, the following findings can be developed:

1. The results demonstrated the applicability of the Taguchi technique and GRA in determining the optimal welding variables for the FSW of aluminum alloy AA5754.
2. The optimal procedure variables for the Taguchi technique optimization and GRA are rotating speed at 1000 rpm, welding speed at 60 mm/min, and tilt angle at  $2.5^\circ$ .
3. The response table of *S/N* ratios demonstrated that rotational speed, which is ranked 1, has a significant impact on the overall mechanical properties of the weld joint, while welding speed and tilt angle are ranked 2 and 3, respectively.
4. Higher tensile strength, hardness, and impact toughness are demonstrated by the results, which have the largest grey relational grade of 1.
5. Hardness enhancement in the weld regions of aluminum alloy AA5754 may be primarily caused by smaller grain

**Fig. 7** Fracture surface of the tensile sample **a** exp.#4, **b** exp.#5, and **c** exp.#6



sizes in the weld region, which may be related to the dynamic recrystallization phenomenon.

6. The predicted optimal welding setting produced maximum values for the following properties: tensile strength of 136 Mpa, hardness of 85.25 HV, and impact toughness of 13 J.
7. Friction stir welding is an easy and inexpensive welding process that is used in a variety of industries, including aerospace, automotive, and marine.

**Author contribution** All the authors have read and agreed with the research presented.

**Funding** Open access funding provided by The Science, Technology & Innovation Funding Authority (STDF) in cooperation with The Egyptian Knowledge Bank (EKB).

**Data and code availability** Not applicable.

## Declarations

**Ethical approval** Not applicable.

**Conflict of interest** The authors declare no competing interests.

**Open Access** This article is licensed under a Creative Commons Attribution 4.0 International License, which permits use, sharing, adaptation, distribution and reproduction in any medium or format, as long as you give appropriate credit to the original author(s) and the source, provide a link to the Creative Commons licence, and indicate if changes were made. The images or other third party material in this article are included in the article's Creative Commons licence, unless indicated otherwise in a credit line to the material. If material is not included in the article's Creative Commons licence and your intended use is not permitted by statutory regulation or exceeds the permitted use, you will need to obtain permission directly from the copyright holder. To view a copy of this licence, visit <http://creativecommons.org/licenses/by/4.0/>.

## References

1. Hirsch J (2014) Recent development in aluminum for automotive applications. *Trans Nonferrous Met Soc China* 24:1995–2002
2. Ma SC, Zhao Y, Zou JS, Yan K, Liu C (2017) The effect of laser surface melting on microstructure and corrosion behavior of friction stir welded aluminum alloy 2219. *Opt Laser Technol* 96:299–306
3. Dursun T, Soutis C (2014) Recent developments in advanced aircraft aluminum alloys. *Mater Des* 56:862–871
4. Threadgill PL, Leonard AJ, Shercli HR, Withers PJ (2009) Friction stir welding of aluminium alloys. *Int Mater Rev* 54:49–93
5. Nandan R, DebRoy T, Bhadeshia HKDH (2008) Recent advances in friction-stir welding—process, weldment structure and properties. *Prog Mater Sci* 53:980–1023
6. Kashaev N, Ventzke V, Cam G (2018) Prospects of laser beam welding and friction stir welding processes for aluminum airframe structural applications. *J Manuf Process* 36:571–600
7. Abbasi M, Givi M, Bagheri B (2020) New method to enhance the mechanical characteristics of Al-5052 alloy weldment produced by tungsten inert gas. *Proc Inst Mech Eng, Part B: J Eng Manuf* 0(0). <https://doi.org/10.1177/0954405420929777>
8. Abdollahzadeh A, Bagheri B, Abbasi M, Sharifi F, Mirsalehi SE, Moghaddam AO (2021) A modified version of friction stir welding process of aluminum alloys: analyzing the thermal treatment and wear behavior. *Proc Inst Mech Eng Part L: J Mater Des Appl* 235:2291–3230
9. Abbasi M, Abdollahzadeh A, Bagheri B, Ostovari Moghaddam A, Sharifi F, Dadaei M (2021) Study on the effect of the welding environment on the dynamic recrystallization phenomenon and residual stresses during the friction stir welding process of aluminum alloy. *Proc Inst Mech Eng Part L: J Mater Des Appl* 235:1809–1826
10. Rajakumar S, Balasubramanian V (2012) Predicting grain size and tensile strength of friction stir welded joints of AA7075-T6 aluminium alloy. *Mater Manuf Process* 27:78–83
11. Singh A, Kumar V, Grover NK (2019) A study of microstructure and mechanical properties of friction stir welding aluminium alloy AA6082 with Zn interlayer. *Mater Res Express* 6:116596
12. Raja R, Jannet S, Mohanasundaram S (2022) Multi response optimization of process parameters of friction stir welded AA6061 T6 and AA 7075 T651 using response surface methodology. *J Sci Ind Res* 73:232–234
13. Rajendran C, Srinivasan K, Balasubramanian V, Balaji H, Selvaraj P (2019) Identifying combination of friction stir welding parameters to maximize strength of lap joints of AA2014-T6 aluminum alloy. *Aust J Mech Eng* 17:64–75
14. Tariq M, Khan I, Hussain G, Farooq U (2019) Microstructure and micro-hardness analysis of friction stir welded bi-layered laminated aluminum sheets. *Int J Lightweight Mater Manufact* 2:123–130
15. Shen Z, Ding Y, Chen J, Fu L, Liu XC, Chen H, Guo W, Gerlich AP (2019) Microstructure, static and fatigue properties of refill friction stir spot welded 7075–T6 aluminium alloy using a modified tool. *Sci Technol Weld Join* 24:587–600
16. Gomathisankar M, Gangatharan M, Pitchipoo P (2018) A novel optimization of friction stir welding process parameters on aluminum alloy 6061–T6. *Mater Today: Proceedings* 5:14397–14404
17. Fathi J, Ebrahimzadeh P, Farasati R, Teimouri R (2019) Friction stir welding of aluminum 6061–T6 in presence of water cooling: analyzing mechanical properties and residual stress distribution. *Int J Lightweight Mater Manufact* 2:107–115
18. Abdollahzadeh A, Bagheri B, Abbasi M, Kokabi AH, Moghaddam AO (2021) Comparison of the weldability of AA6061-T6 joint under different friction stir welding conditions. *J Mater Eng Perform* 30:1110–1127
19. Hadji I, Badji R, Gaceb M, Cheniti B (2022) Dissimilar FSW of AA2024 and AA7075: effect of materials positioning and tool deviation value on microstructure, global and local mechanical behavior. *Int J Adv Manuf Technol* 118:2391–2403
20. Panda MR, Mahapatraand SS, Mohanty CP (2015) Parametric investigation of friction stir welding on AA6061 using Taguchi technique. *Materials Today: Proceedings* 2:2399–2406
21. Devaiah D, Kishore K, Laxminarayana P (2017) Parametric optimization of friction stir welding parameters using Taguchi technique for dissimilar aluminum alloys (AA5083 and AA6061). *Int Organ Sci Res* 7:44–49
22. Panda MR, Mahapatraand SS, Mohanty CP (2015) Parametric investigation of friction stir welding on AA6061 using Taguchi technique. *Mater Today: Proc* 22:399–2406
23. Shah LH, Zainal Ariffin NF, Razali AR (2015) Parameter optimization of AA6061-AA7075 dissimilar friction stir welding using the Taguchi method. *Appl Mech Mater* 695:20–23

24. Bhojan N, Senthilkumar B, Deepanraj B (2016) Parametric influence of friction stir welding on cast Al6061/20%SiC/2%MoS<sub>2</sub> MMC Mechanical Properties. *Appl Mech Mater* 852:297–303
25. Ranjith R (2014) Joining of dissimilar aluminium alloys AA2014 T651 and AA6063 T651 by friction stir welding process. *WSEAS Trans Appl Theor Mech* 9:179–186
26. Palani K, Elanchezian C (2018) Multi response optimization of friction stir welding process parameters in dissimilar alloys using grey relational analysis. *IOP Conf Ser: Mater Sci Eng* 9:179–186
27. Montgomery DC (2017) *Design and analysis of experiments*, John Wiley & Sons
28. Goswami A, Kumar J (2014) Investigation of surface integrity, material removal rate and wire wear ratio for WEDM of Nimonic 80A alloy using GRA and Taguchi method. *Eng Sci Technol Int J* 17:173–184
29. Deepanraj B, Anantha Raman L, Senthilkumar N, Shivasankar J (2020) Investigation and optimization of machining parameters influence on surface roughness in turning AISI 4340 Steel. *FME Trans* 48:383–390
30. Tamizharasan T, Senthilkumar N, Selvakumar V, Dinesh S (2019) Taguchi's methodology of optimizing turning parameters over chip thickness ratio in machining P/M AMMC. *SN Appl Sci* 1:160
31. Senthilkumar N, Tamizharasan T (2012) Impact of interface temperature over flank wear in hard turning using carbide inserts. *Procedia Eng* 38:613–621
32. Dhinakarraj CK, Shivasankar J, Senthilkumar N (2020) Investigations of micro-milling parameters in woven banana fibre reinforced polymer composite filled with rice bran particles. *Int J Veh Struct Syst* 12:150–156
33. Rajendran C, Srinivasan K, Balasubramanian V, Balaji H, Selvaraj P. (2017). Identifying combination of friction stir welding parameters to maximize strength of lap joints of AA2014-T6 aluminum alloy. *Arch Mech Technol Mater* 37:6–21
34. Abbasi M, Bagheri B, Abdollahzadeh A, Moghaddam AO (2021) A different attempt to improve the formability of aluminum tailor welded blanks (TWB) produced by the FSW. *Int J Mater Form* 14:1189–1208
35. Santhanam SKV, Ramaiyan S, Rathinaraj L, Chandran R (2016) Multi response optimization of submerged friction stir welding process parameters using grey relational analysis. *ASME 2016 Int Mech Eng Congr Exposition* 2:11–17
36. Ravikumar S, Rao VS, Pranesh V (2014) Multiple response optimization with grey relational analysis of friction stir welding parameters in joining dissimilar aluminium alloys by Taguchi method. *Appl Mech Mater* 592:555–559
37. Raweni A, Majstorović V, Sedmak A, Tadić S, Kirin S (2018) Optimization of AA5083 friction stir welding parameters using Taguchi method. *Tehnički vjesnik* 25:861–866
38. Senthilkumar N, Ganapathy T, Tamizharasan T (2014) Optimization of machining and geometrical parameters in turning process using Taguchi Method, *Austral. J Mech Eng* 12:233–246
39. Safeen W, Hussain S, Wasim A, Jahanzaib M, Aziz H, Abdalla H (2016) Predicting the tensile strength, impact toughness, and hardness of friction stir-welded AA6061-T6 using response surface methodology. *Int J Adv Manuf Technol* 87:1765–1781
40. Taguchi G (1990) *Introduction to quality engineering*. Asian Productivity Organization, Tokyo
41. Vidal C, Infante V (2013) Optimization of FS welding parameters for improving mechanical behavior of AA2024-T351 joints based on Taguchi method. *J Mater Eng Perform* 22:2261–2270
42. Ramamurthy M, Balasubramanian P (2022) Parametric optimization in friction stir joining of AA2014 and AA6061 alloys through entropy based multiobjective GRA approach. *Mater Today: Proc* 59:1249–1255
43. Kuo Y, Yang T, Huang GW (2008) The use of a grey-based Taguchi method for optimizing multi-response simulation problems. *Eng Optim* 40:517–528
44. Tosun N (2006) Determination of optimum parameters for multi-performance characteristics in drilling by using grey relational analysis. *Int J Adv Manuf Technol* 28:450–455
45. Bozkurt Y (2012) The optimization of friction stir welding process parameters to achieve maximum tensile strength in polyethylene sheets. *Mater Des* 35:440–445
46. Antony J (2014) *Design of experiments for engineers and scientists*. Elsevier, pp 33–50
47. Pachal AS, Bagesar A (2013) Taguchi optimization of process parameters in friction welding of 6061 aluminum alloy and 304 steel: a review. *Int J Emerg Technol Adv Eng* 3:229–233
48. Arbegast WJ (2003) Modeling friction stir joining as a metalworking process. *Proc Hot Aluminum alloys III*:313–327
49. Elangovan K, Balasubramanian V (2007) Influences of pin profile and rotational speed of the tool on the formation of friction stir processing zone in AA2219 aluminium alloy. *Mater Sci Eng A* 459:7–18
50. Mishra RS, Ma ZY (2005) Friction stir welding and processing. *Mater SciEng* 50:1–78
51. Babu S, Elangovan K, Balasubramanian V, Balasubramanian M (2009) Optimizing friction stir welding parameters to maximize tensile strength of AA2219 aluminum alloy joints. *Met Mater Int* 15:321–330
52. Ahmadkhaniha D, Heydarzadeh Sohi M, Zarei-Hanzaki A, Bayazid SM, Saba M (2015) Taguchi optimization of process parameters in friction stir processing of pure Mg. *J Magnes Alloy* 3:168–172
53. Wen Q, Li W, Patel V, Gao Y, Vairis A (2020) Investigation on the effects of welding speed on bobbin tool friction stir welding of 2219 aluminum alloy. *Met Mater Int* 26:1830–1840
54. Shojaeefard MH, Akbari M, Khalkhali A, Asadi P, Parivar AH (2014) Optimization of microstructural and mechanical properties of friction stir welding using the cellular automaton and Taguchi method. *Mater Des* 64:660–666
55. Meran C, Canyurt OE (2010) Friction stir welding of austenitic stainless steels. *J Achiev Mater Manuf Eng* 43:432–439
56. Jafari M, Abbasi M, Poursina D, Gheysarian A, Bagheri B (2017) Microstructures and mechanical properties of friction stir welded dissimilar steel-copper joints. *J Mech Sci Technol* 31:1135–1142
57. Dehghani M, Akbarimousavi SAA, Amadeh A (2013) Effects of welding parameters and tool geometry on properties of 3003-H18 aluminum alloy to mild steel friction stir weld. *T Nonfer Metal Soc* 23:1957–1965
58. Rathinasuriyan C, Kumar VSS (2020) Optimisation of submerged friction stir welding parameters of aluminium alloy using RSM and GRA. *Adv Mater Process Technol* 7:1–14
59. Wang FF, Li WY, Shen J, Hu SY, Dos Santos JF (2015) Effect of tool rotational speed on the microstructure and mechanical properties of bobbin tool friction stir welding of Al-Li alloy. *Mater Des* 86:933–940
60. Sutton MA, Yang B, Reynolds AP, Taylor R (2002) Microstructural studies of friction stir welds in 2024-T3 aluminum. *Mater Sci Eng, A* 323:160–166
61. Bagheri B, Abdollahzadeh A, Abbasi M, Kokabi AH (2021) Effect of vibration on machining and mechanical properties of AZ91 alloy during FSP: modeling and experiments. *Int J Mater Form* 14:623–640
62. Bagheri B, Sharifi F, Abbasi M, Abdollahzadeh A (2022) On the role of input welding parameters on the microstructure and mechanical properties of Al6061-T6 alloy during the friction stir welding: experimental and numerical investigation. *Proc Inst Mech Eng Part L: J Mater Des Appl* 236:299–318
63. Bagheri B, Shamsipur A, Abdollah Zadeh A, Mirsalehi SE (2023) Investigation of SiC nanoparticle size and distribution effects on microstructure and mechanical properties of Al/SiC/Cu composite during the FSSW process: experimental and simulation. *Met Mater Int* 29:1095–1112

64. Rizi VS, Abbasi M, Bagheri B (2021) Investigation into micro-structure and mechanical behaviors of joints made by friction stir vibration brazing between low carbon steels. *Phys Scr* 96:125704
65. Zhai M, Wu C, Su H (2020) Influence of tool tilt angle on heat transfer and material flow in friction stir welding. *J Manuf Process* 59:98–112
66. Wahid M A, Siddiquee AN, Khan ZA, Asjad M (2016) Friction stir welds of Al alloy-Cu. An investigation on effect of plunge depth. *Arch Mech Eng* 63:619–634
67. Bagheri B, Abbasi M, Hamzeloo R (2021) Comparison of different welding methods on mechanical properties and formability behaviors of tailor welded blanks (TWB) made from AA6061 alloys. *Proc Inst Mech Eng C J Mech Eng Sci* 235:2225–2237

**Publisher's Note** Springer Nature remains neutral with regard to jurisdictional claims in published maps and institutional affiliations.